

Theory of four-point alternating current potential drop measurements on a metal half-space

Nicola Bowler

Center for Nondestructive Evaluation, Iowa State University, Applied Sciences Complex II, Ames, IA 50011, USA

E-mail: nbowler@iastate.edu

Received 13 September 2005, in final form 4 December 2005

Published 20 January 2006

Online at stacks.iop.org/JPhysD/39/584

Abstract

An analytic expression describing the complex voltage measured between the pickup points of a four-point probe, in contact with the surface of a half-space conductor, is derived. The driving current is assumed to be time harmonic. There are two contributions to the measured voltage. One arises from the potential drop due to electric current flowing in the conductor. The other arises from induction in the loop of the pickup circuit. Both terms are obtained by integrating analytic expressions for the electric field, derived previously, along appropriate paths. Theory is compared with experimental data for co-linear and rectangular arrangements of the probe points, and very good agreement is obtained.

1. Introduction

Four-point direct current potential drop (DCPD) methods for the measurement of material conductivity are well established in the fields of geophysics [1, 2], semiconductor characterization [3] and nondestructive evaluation [4, 5]. Alternating current potential drop (ACPD) measurements permit additional, depth-dependent information to be obtained through the phenomenon of the electromagnetic skin effect, in which the current is confined to flow in a ‘skin’ at the surface of the conductor, whose depth is approximately inversely proportional to the square root of the excitation frequency. The ACPD technique therefore has application in assessing materials whose electromagnetic parameters vary with depth, for example, in the case of electrically conductive surface treatments and coatings. From a practical point of view, an advantage of ACPD over DCPD is that a lower measuring current can be applied in order to achieve a given sensitivity [4] (section 8). This reduces the risk of heating of the specimen and associated changes in electrical conductivity.

In previous work, Mitrofanov has derived an expression for the complex voltage measured between the pickup points of a four-point probe, in contact with the surface of a half-space conductor [6]. The solution was expressed in terms of

an infinite series expansion in powers of k , where

$$k = \frac{1+i}{\delta} \quad \text{with } \delta = \left(\frac{2}{\omega\mu\sigma}\right)^{1/2}, \quad (1)$$

δ being the electromagnetic skin depth in the conductor. In equation (1), $\omega = 2\pi f$ is the angular frequency of the injected current and μ and σ are the magnetic permeability and electrical conductivity of the half-space, respectively.

Here, an analytic expression describing the complex voltage measured between the pickup points of a four-point probe, in contact with the surface of a half-space conductor, is derived in closed form. There are two contributions to the measured voltage. One arises from the potential drop due to electric current flowing in the conductor. The other arises from induction in the loop of the pickup circuit. Both terms are obtained by integrating analytic expressions for the electric field, derived previously [7, 8], along appropriate paths. It is shown that the closed-form expression obtained here for the potential drop due to current flowing in the conductor can be expressed as a power series in k , giving the same result as that presented in [6]. The contribution to the measured complex voltage due to inductance in the pickup circuit was not analysed in [6].

Theory is compared with experimental data for co-linear and rectangular arrangements of the four probe points in

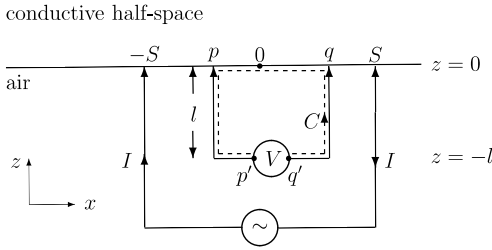


Figure 1. Four point probe in contact with a conductive half-space. The path of integration, C (---), may occupy any plane of constant y . Here the plane $y = 0$ is shown. l is the dimension of the pickup circuit perpendicular to the conductor surface.

contact with a thick aluminium block and very good agreement is obtained in both cases.

2. Analysis

The ACPD method measures a complex voltage, V , which has two contributions:

$$V = v + \varepsilon. \quad (2)$$

The first term, v , is the potential drop between the two points on the plate at which the measurement circuit makes contact with its surface. The source of v is the current in the plate injected by the other two points of the four-point probe. At arbitrary frequency, v is complex. The second contribution, ε , is proportional to the inductance of the measurement circuit. It arises from the changing magnetic flux within the loop of the measurement circuit due to harmonic variation of the applied current, of the form $e^{-i\omega t}$. ε is purely inductive, therefore imaginary. In the static limit of direct current, only v remains. For the geometry given in figure 1,

$$v = \int_{(q,0,0)}^{(p,0,0)} \mathbf{E} \cdot d\mathbf{l}, \quad (3)$$

and

$$\varepsilon = \oint_C \mathbf{E} \cdot d\mathbf{l}, \quad (4)$$

where C is a closed loop in the case where p' and q' coincide, as happens when the pickup wires are twisted together at their point of meeting. At low frequency, the measured potential drop is almost exclusively due to the conductor. In an ACPD measurement on a conductive plate, the contribution to V from the plate is most significant at lower frequencies, with the contribution from ε becoming larger, and eventually dominant, as the frequency increases. Strictly, the quantities V , v , ε and \mathbf{E} are complex amplitudes. For brevity, the time dependence is not shown explicitly in equations (2) to (4) or in the equations that follow.

2.1. Electric field

For current injected into a half-space conductor by a single wire held perpendicular to the conductor surface, the components of the electric field in the conductor are [7]

$$E_\rho^s(\mathbf{r}) = -\frac{I}{2\pi\sigma} \frac{ik}{\rho} \left\{ e^{ikz} - \frac{e^{ikr}}{ikr} \left[1 + \frac{(ikz)^2}{ikr} \left(1 - \frac{1}{ikr} \right) \right] \right\}, \quad z > 0, \quad (5)$$

$$E_z^s(\mathbf{r}) = \frac{I}{2\pi\sigma} \frac{z}{r^3} e^{ikr} (1 - ikr), \quad z > 0, \quad (6)$$

in which ρ and z are the variables of a cylindrical co-ordinate system centred on the current wire and $r^2 = \rho^2 + z^2$. The electric field in air may be expressed [8] as

$$\mathbf{E}^s = \mathbf{E}^w + \mathbf{E}^c, \quad \rho > 0, z \leq 0, \quad (7)$$

where

$$\mathbf{E}^w = \hat{z} \frac{I}{2\pi} i\omega\mu_0 \ln \rho, \quad \rho > 0, z \leq 0 \quad (8)$$

and

$$\mathbf{E}^c = \frac{I}{2\pi\sigma} \int_0^\infty \gamma e^{\kappa z} [\hat{\rho} J_1(\kappa\rho) - \hat{z} J_0(\kappa\rho)] d\kappa, \quad z \leq 0. \quad (9)$$

In equation (9), $\gamma^2 = \kappa^2 - k^2$ and $J_i(x)$ is the i -th-order Bessel function of the first kind. \mathbf{E}^w is the electric field in air due to the current flowing in the injection wire. \mathbf{E}^c is the electric field in air due to the current flowing in the half-space conductor.

For a system of two current-carrying wires in contact with the metal surface at co-ordinates $(\pm S, 0, 0)$, as shown in figure 1, the electric field \mathbf{E} can be obtained by the superposition of the field due to a single wire, \mathbf{E}^s , whose components are given above:

$$\mathbf{E}(\mathbf{r}) = \mathbf{E}^s(\mathbf{r}_+) - \mathbf{E}^s(\mathbf{r}_-) \quad (10)$$

with $r_\pm = \sqrt{(x \pm S)^2 + y^2 + z^2}$.

2.2. Calculation of v

2.2.1. Closed form. In general, the line of the pickup points may be off-set from the line of the current injection points. Let $y = c = \text{constant}$ and then choose the path of the integral in equation (3) such that

$$v = - \int_p^q E_x(x, c, 0) dx. \quad (11)$$

Now,

$$E_x(x, c, 0) = \frac{(x+S)}{\rho_+} E_\rho^s(\rho_+, 0) - \frac{(x-S)}{\rho_-} E_\rho^s(\rho_-, 0), \quad (12)$$

where $\rho_\pm = \sqrt{(x \pm S)^2 + c^2}$. Combining the above two equations and making the change of variable $X = x \pm S$ gives

$$v = -I_+ + I_-, \quad (13)$$

where

$$I_\pm = \int_{p \pm S}^{q \pm S} \frac{X}{\sqrt{X^2 + c^2}} E_\rho^s(X, c, 0) dX. \quad (14)$$

Putting $E_\rho^s(X, c, 0)$ from equation (5) into the integrand of equation (14) gives

$$I_\pm = -\frac{ikI}{2\pi\sigma} \int_{p \pm S}^{q \pm S} \left[\frac{X}{X^2 + c^2} - \frac{X e^{ik\sqrt{X^2 + c^2}}}{ik(X^2 + c^2)^{3/2}} \right] dX. \quad (15)$$

Integration of the first term in equation (15) is straightforward. The second term in equation (15) may be evaluated by making a further change of variable, $\alpha = \sqrt{X^2 + c^2}$, and using the following identity (equation (2.325.2) in [9]):

$$\int \frac{e^{ax}}{x^2} dx = -\frac{e^{ax}}{x} - aE_1(-ax), \quad (16)$$

in which $E_1(z)$ is the exponential integral function, defined (equation (5.1.1) in [10]) as

$$E_1(z) = \int_z^\infty \frac{e^{-t}}{t} dt, \quad |\arg z| < \pi. \quad (17)$$

Ultimately, the following expression for v is obtained:

$$v = \frac{I}{2\pi\sigma} [f_i(S+q, c) - f_i(S-q, c) - f_i(S+p, c) + f_i(S-p, c)], \quad (18)$$

where, as will be shown subsequently, $f_i(x, y)$ can take several forms. In exact, closed form,

$$\begin{aligned} f_{\text{exact}}(x, y) &= f_{\text{exact}}(\rho = \sqrt{x^2 + y^2}) \\ &= \frac{e^{ik\rho}}{\rho} + ik[\ln \rho + E_1(-ik\rho)]. \end{aligned} \quad (19)$$

2.2.2. Series form. The result presented in equations (18) and (19) can be expressed in terms of a power series in k . In this way it can be shown that the result is in agreement with that of an independent calculation [6]. The two relations (equations (4.2.1) and (5.1.11) in [10])

$$e^z = \sum_{n=0}^{\infty} \frac{z^n}{n!}, \quad (20)$$

$$E_1(z) = -\gamma_e - \ln z - \sum_{n=1}^{\infty} \frac{(-1)^n z^n}{nn!}, \quad |\arg z| < \pi, \quad (21)$$

applied to the exponential and exponential integral functions in equation (19) give

$$f_{\text{exact}}(\rho) = -ik[\gamma_e + \ln(-ik) - 1] + f_{\text{series}}(\rho) \quad (22)$$

in which $\gamma_e = 0.577\,216\dots$ is Euler's constant and

$$f_{\text{series}}(\rho) = \frac{1}{\rho} \left[1 - \sum_{n=1}^{\infty} \frac{(ik\rho)^{n+1}}{n(n+1)!} \right]. \quad (23)$$

Note that the terms present in the relation between f_{exact} and f_{series} (equation (22)) are independent of ρ . This means that they drop out when inserted into equation (18). Hence f_{series} (equation (23)) may be inserted directly into equation (18) as an alternative to f_{exact} (equation (19)). The resulting series representation for v given by combining equations (18) and (23) agrees with that presented in [6].

2.2.3. Special cases. One commonly-used probe configuration is that in which the four probe points are arranged along a straight line, with the voltage pickup points positioned symmetrically about the midpoint between the current injection points. In the case of this co-linear, symmetric probe, $p = -q$ and $c = 0$. Equation (18) reduces to

$$v^{\text{LS}} = \frac{I}{\pi\sigma} [f_i(S+q, 0) - f_i(S-q, 0)]. \quad (24)$$

For a rectangular probe configuration, in which the line between the current injection points forms one side of the rectangle and that between the voltage pickup points forms the opposite side, $p = -S$ and $q = S$ so that

$$v^{\text{R}} = \frac{I}{\pi\sigma} [f_i(2S, c) - f_i(0, c)]. \quad (25)$$

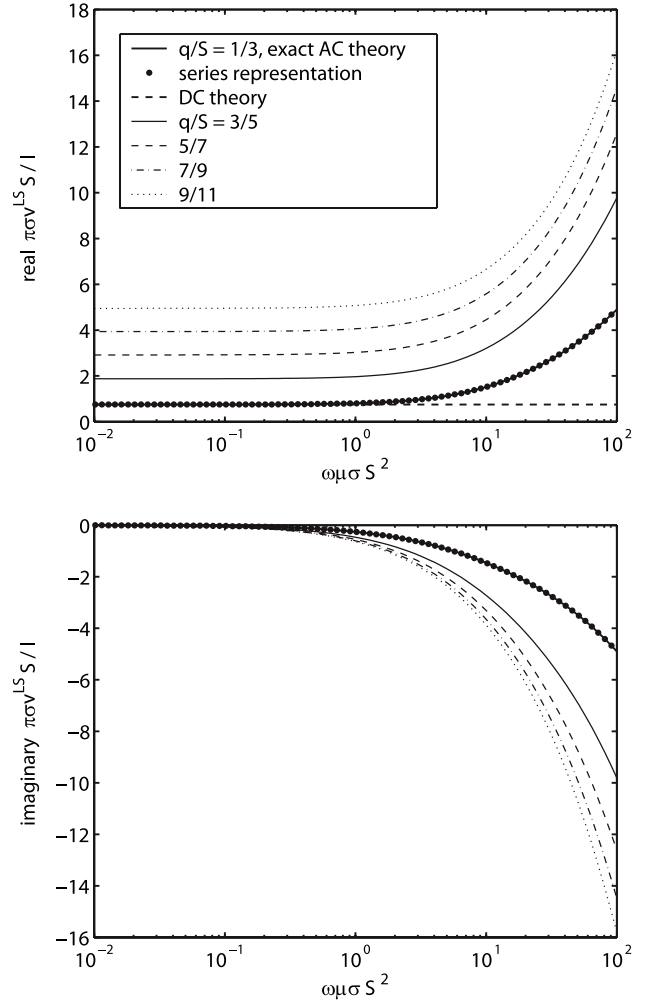


Figure 2. Dimensionless pickup voltage, $\pi\sigma v^{\text{LS}}S/I$, as a function of dimensionless frequency, $\omega\mu\sigma S^2$, in the case of a co-linear, symmetric probe, for $q/S = 1/3(0.333)$, $3/5(0.600)$, $5/7(0.714)$, $7/9(0.778)$ and $9/11(0.818)$.

In the limit of direct current, $k \rightarrow 0$ and

$$f_{\text{exact}}^{\text{DC}}(\rho) = f_{\text{series}}^{\text{DC}}(\rho) = \frac{1}{\rho}, \quad (26)$$

in agreement with results presented in [3, 5, 11].

In figure 2, the real and imaginary parts of the dimensionless voltage, $\pi\sigma v^{\text{LS}}S/I$, are plotted versus dimensionless frequency, $\omega\mu\sigma S^2$, for various values of the ratio of pickup length to current injection length, q/S , for a co-linear, symmetric probe. It can be seen that the voltage increases as the pickup points approach the current injection points more closely, i.e. as q/S increases. Voltage values calculated using the series representation for v , equation (23), are also shown for the probe with equally-spaced probe points, $q/S = 1/3$. To achieve agreement to within 2% of values calculated using the exact solution at the highest frequency considered, 30 terms in the series are required. As q/S increases, yet more terms are needed.

In figure 3, the real and imaginary parts of the dimensionless voltage, $\pi\sigma v^{\text{R}}S/I$, are plotted versus dimensionless frequency, $\omega\mu\sigma S^2$, for various values of the

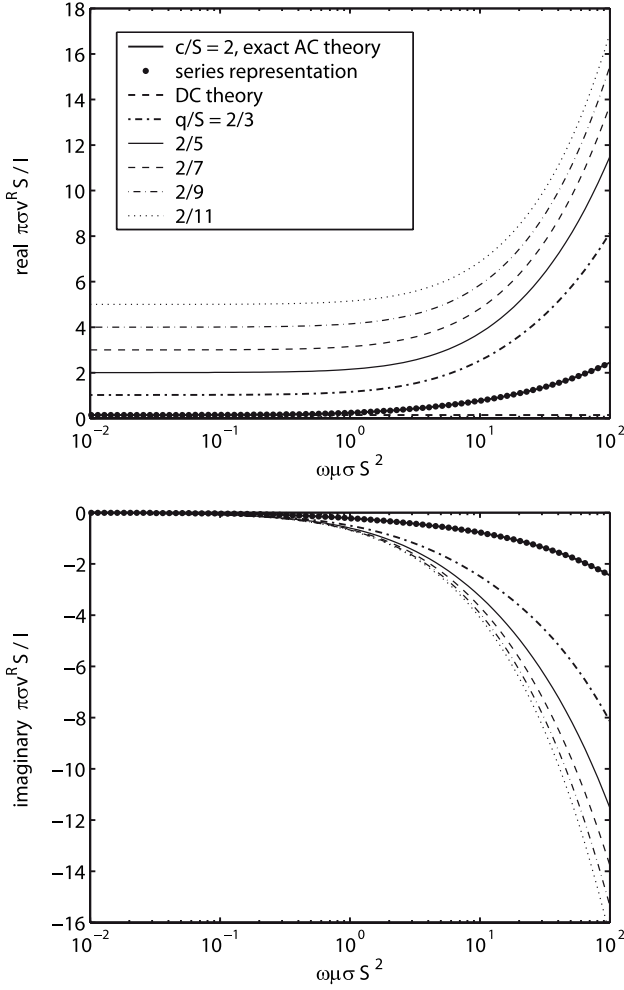


Figure 3. Dimensionless pickup voltage, $\pi\sigma v^R S/I$, as a function of dimensionless frequency, $\omega\mu\sigma S^2$, in the case of a rectangular probe, for $c/S = 2, 2/3$ (0.667), $2/5$ (0.400), $2/7$ (0.286), $2/9$ (0.222) and $2/11$ (0.182).

aspect ratio of a rectangular probe, $c/(2S)$. Again, the pickup voltage increases as the pickup points approach the current injection points more closely, i.e. as c/S decreases. To achieve agreement within 2% between values calculated using the exact solution (equation (19)) and the series solution (equation (23)) for a square-head probe ($c/S = 2$) at the highest frequency considered, 70 terms in the series are required.

In both figures 2 and 3 it is evident that, below a certain frequency, the pickup voltage is approximately real and constant. In this low-frequency regime, the measured voltage matches that obtained in the dc limit and equation (26) applies. Hence, in the low-frequency regime, v is independent of μ , and σ may be determined independently of μ by adjusting the value of σ until theory matches low-frequency experimental data. Once σ is known, μ may be determined by fitting theory with experimental data taken at higher frequencies. This procedure is demonstrated in [12] in characterizing metal plates which are somewhat thinner than the probe length [13].

Comparing results shown in figures 2 and 3 it can be seen that the co-linear and rectangular probes perform more similarly as the pickup points approach the current injection points more closely, as is to be expected.

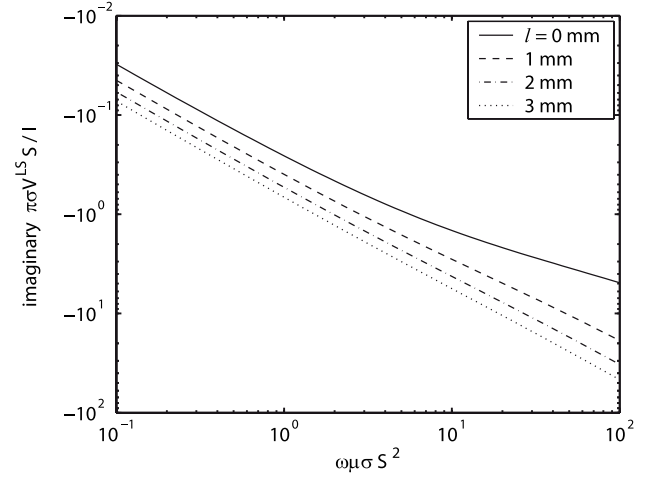


Figure 4. Imaginary part of the dimensionless pickup voltage, $\pi\sigma V^{LS} S/I$, as a function of dimensionless frequency, $\omega\mu\sigma S^2$, in the case of a co-linear, symmetric probe, with $q/S = 1/3$. Curves are plotted for various values of the parameter l , the height of the pickup loop above the conductor surface (figure 1). The area of the pickup loop, and hence the inductance of the loop, is proportional to l .

2.3. Calculation of ε

It can easily be shown that \mathbf{E}^c (equation (9)) is conservative ($\nabla \times \mathbf{E}^c = 0$) and therefore does not contribute to the integral around the closed loop from which ε is derived (equation (4)). Hence, with equations (7) and (10),

$$\varepsilon = \oint_C [\mathbf{E}^w(\mathbf{r}_+) - \mathbf{E}^w(\mathbf{r}_-)] \cdot d\mathbf{l}. \quad (27)$$

Considering the form of \mathbf{E}^w (equation (8)) evaluation of the integral in equation (27) is straightforward, yielding

$$\varepsilon = \frac{I}{2\pi} i\omega\mu_0 l \ln \left[\frac{\sqrt{(S+q)^2 + c^2} \sqrt{(S-p)^2 + c^2}}{\sqrt{(S-q)^2 + c^2} \sqrt{(S+p)^2 + c^2}} \right]. \quad (28)$$

The self-inductance of the pickup circuit, L , may therefore be expressed as

$$L = \frac{I}{2\pi} \mu_0 l \ln \left[\frac{\sqrt{(S+q)^2 + c^2} \sqrt{(S-p)^2 + c^2}}{\sqrt{(S-q)^2 + c^2} \sqrt{(S+p)^2 + c^2}} \right]. \quad (29)$$

2.4. Complex voltage V

Combining results (18) and (28) in accordance with equation (2) gives, finally,

$$V = \frac{I}{2\pi\sigma} [F(S+q, c) - F(S-q, c) - F(S+p, c) + F(S-p, c)], \quad (30)$$

where

$$F(x, y) = F(\rho = \sqrt{x^2 + y^2}) = \frac{e^{ik\rho}}{\rho} + ik \left[\left(1 - \frac{ikl}{\mu_r}\right) \ln \rho + E_1(-ik\rho) \right], \quad (31)$$

and $\mu_r = \mu/\mu_0$ is the relative permeability of the half-space.

Table 1. Probe parameters.

Configuration	S (mm)	p (mm)	q (mm)	c (mm)	l (mm) (fitted value)
Co-linear	20.03 ± 0.07	-17.5 ± 0.2	17.6 ± 0.4	0	2.98 ± 0.01
Rectangular	17.64 ± 0.07	-17.47 ± 0.07	17.55 ± 0.07	2.5 ± 0.2	2.15 ± 0.01

Table 2. Half-space parameters conductivity, σ , thickness, T and lateral dimensions, $w \times d$.

Metal	Alloy	σ (MSm ⁻¹)	T (mm)	$w \times d$ (mm)
Aluminium	2024	17.6 ± 0.2	101	149×202

In figure 4 the effect of varying l on V is shown in the case of a co-linear, symmetric probe with equally-spaced probe points ($q/S = 1/3$). Only the imaginary part of V is shown since ε is purely imaginary and has no influence on the real part of V . It can be seen that, as l increases, $\text{Im}(V)$ becomes linear in frequency due to the dominance of $|\varepsilon|$ over $|\text{Im}(v)|$. From a practical point of view, it is important to minimize l so that the component of V which carries information about the specimen, v , is not swamped by the inductive term, ε .

3. Experiment

In this section, the theoretical expression for the complex voltage (equations (30) and (31)) is validated by comparison with experimental data. Two different four-point probes, one with co-linear arrangement of the probe points and one rectangular, were used. The probes were constructed by mounting four sprung, point contacts in a plastic support block. The separation of the contacts was measured using digital callipers. With reference to figure 1, the dimensions of the probe are listed in table 1. The uncertainty in the dimensions derives primarily from some lateral play in the pin position which can occur as the springs are compressed. Measurements of complex voltage were made with the probes in contact with a thick, alloy 2024 aluminium block, whose parameters are listed in table 2. The conductivity of the block was measured independently using an eddy-current coil. Details of the conductivity measurement and further details of the experimental procedure for the ACPD measurements can be found in [12, 14].

The dimensions of the aluminium block, with respect to the dimensions of the probes, are such that some discrepancy between theory and experiment due to edge effects is expected. For the co-linear probe placed centrally on the largest face of the aluminium block, the error due to edge effects is minimized by orienting the line of the probe so that it is parallel with the shorter side of the block face ($w = 149$ mm) [4, 15]. The error is also reduced by employing a probe in which the four points are not equally-spaced, but in which the pickup points are closer to the current injection points. In fact, for the co-linear probe used in this experiment, $(q - p)/(2S) \approx 0.88$ and $w/(2S) \approx 3.7$. For these ratios, and assuming that the aluminium block is ‘infinite’ in the direction perpendicular to the line of the probe (dimension d), edge effects are expected to lead to a discrepancy of approximately 2% between theory and experiment in the dc limit [15]. Since in practice this block is finite in the direction perpendicular to the line of the probe

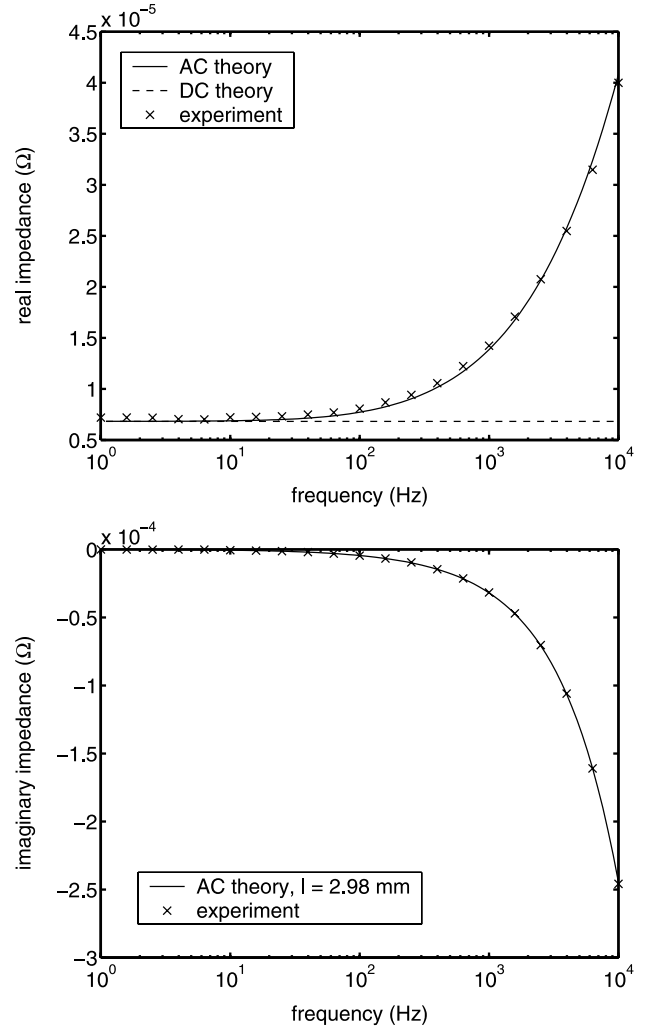


Figure 5. Impedance (V/I) measured by a co-linear, four-point probe (table 1) in contact with an aluminium block (table 2), compared with theory expressed in equation (30), as a function of frequency.

($d = 202$ mm), a discrepancy a little larger than 2% is expected between theory and experiment in the dc limit, becoming smaller as frequency increases, due to greater confinement of the electric field in the region of the probe. According to calculations of DCPD as a function of the ratio of plate thickness to probe dimension (here $T/S \approx 5$) [13], the thickness of the block is expected to approximate a half-space very well, with no significant error arising due to its finite thickness.

Experimental measurements made with co-linear and rectangular probes are compared with theory in figures 5 and 6, respectively. In both cases there is very good agreement between theory and experimental data. The calculated curves shown for the imaginary part of the impedance have been

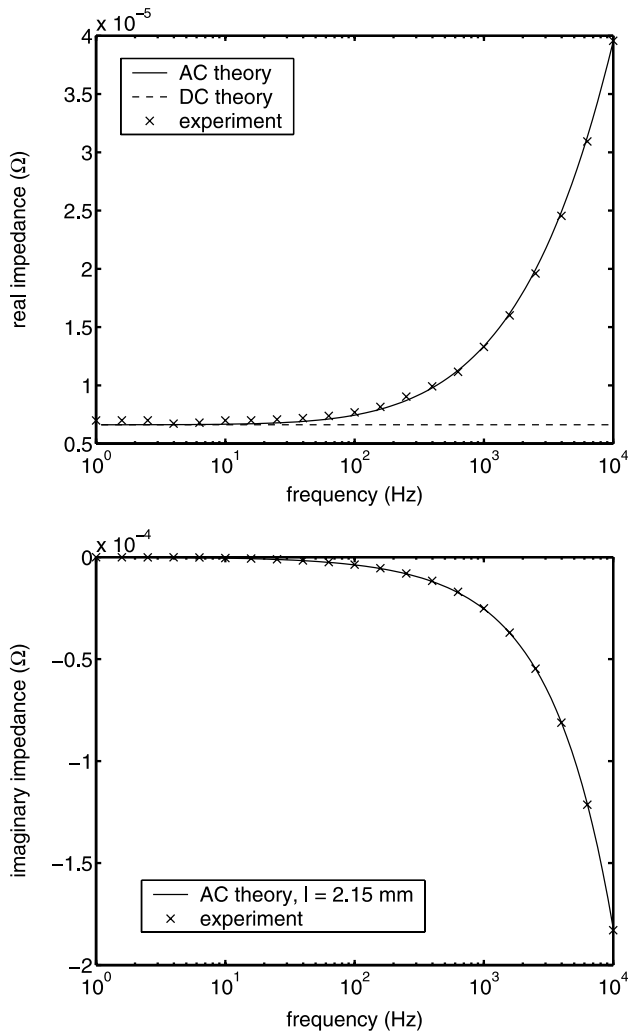


Figure 6. Impedance (V/I) measured by a rectangular, four-point probe (table 1) in contact with an aluminium block (table 2), compared with theory expressed in equation (30), as a function of frequency.

obtained by adjusting the value of the vertical dimension of the pickup circuit, l (see figure 1), to give the best fit to the experimental data. For the co-linear probe, $l = 2.98$ mm. For the rectangular probe, $l = 2.15$ mm. Both these values are similar to the physical values of l for these probes. No free parameters are involved in obtaining the theoretical curves for the real part of the impedance shown in figures 5 and 6. The discrepancy between theory and experiment in the low-frequency regime is approximately 4% for both sets of measurements. The fact that the measured real part of V is larger than that predicted by theory, rather than smaller, indicates that edge effects are likely responsible for the discrepancy. Other significant sources of error are the

uncertainty in the probe dimensions and in the conductivity of the sample. For a full discussion of uncertainties associated with this measurement method, see [14].

4. Conclusion

An exact solution for the complex, frequency-dependent voltage measured between the pickup points of a four-point probe in contact with a metal half-space has been derived. Very good agreement between theory and experiment on an aluminium block has been obtained, for co-linear and rectangular arrangements of the four probe points. As well as providing a method for measuring electrical conductivity and effective magnetic permeability of thick metal specimens, this work forms a foundation for theoretical analysis of four-point ACPD on stratified planar conductors, for the practical purpose of nondestructive evaluation of conductive surface treatments and coatings.

Acknowledgments

This work was supported by the NSF Industry/University Cooperative Research program. The author thanks J T Brown for assistance with the experiments.

References

- [1] Reynolds J M 1997 *Introduction to Applied and Environmental Geophysics* (Chichester: Wiley)
- [2] Parasnis D S 1997 *Principles of Applied Geophysics* 5th edn (London: Chapman and Hall)
- [3] Schroder D K 1998 *Semiconductor Material and Device Characterization* (New York: Wiley)
- [4] Moore P O and McIntire P (ed) Stanley R K (technical ed) 1995 *Nondestructive Testing Handbook (Special Nondestructive Testing Methods vol 9)* 2nd edn (Columbus: American Society of Nondestructive Testing)
- [5] Moore P O (ed) and Udpa S S (technical ed) 2004 *Nondestructive Testing Handbook (Electromagnetic Testing vol 5)* 3rd edn (Columbus: American Society of Nondestructive Testing)
- [6] Mitrofanov V A 1998 *Russ. J. Nondestr. Test.* **34** 183–9
- [7] Bowler N 2004 *J. Appl. Phys.* **95** 344–8
- [8] Bowler N 2004 *J. Appl. Phys.* **96** 4607–13
- [9] Gradshteyn I S and Ryzhik I M (ed) 2000 *Table of Integrals, Series and Products* 6th edn (London: Academic)
- [10] Abramowitz M and Stegun I A (ed) 1972 *Handbook of Mathematical Functions with Formulas, Graphs, and Mathematical Tables* (New York: Dover)
- [11] Uhler A Jr 1955 *Bell Syst. Tech. J.* **34** 105–28
- [12] Bowler N and Huang Y 2005 *IEEE Trans. Magn.* **41** 2102–10
- [13] Bowler N 2005 *Res. Nondestr. Eval.* submitted
- [14] Bowler N and Huang Y 2005 *Meas. Sci. Technol.* **16** 2193–200
- [15] Bowler N and Huang Y 2005 Four-point alternating current potential drop measurements on metal plates: experiment and interpretation, internal document